THE JOURNAL OF PHYSICAL CHEMISTRY C

Article

pubs.acs.org/JPCC

Cu–TiO_2 Hybrid Nanoparticles Exhibiting Tunable Photochromic Behavior

D. M. Tobaldi,*[,†] N. Rozman,[‡] M. Leoni,[§] M. P. Seabra,[†] A. S. Škapin,[‡] R. C. Pullar,*[,†] and J. A. Labrincha[†]

[†]Department of Materials and Ceramic Engineering/CICECO–Aveiro Institute of Materials, University of Aveiro, Campus Universitário de Santiago, 3810-193 Aveiro, Portugal

[‡]Slovenian National Building and Civil Engineering Institute, ZAG, Dimičeva 12, SI-1000 Ljubljana, Slovenia

[§]Department of Civil, Environmental and Mechanical Engineering, University of Trento, Via Mesiano 77, 38123 Trento, Italy

Supporting Information

ABSTRACT: Pure and copper-modified photocatalytic TiO_2 nanopowders were prepared via a green sol–gel route and heated to 450 °C. Copper does not enter the TiO_2 lattice but forms as smaller ∼2 nm Cu-based nanocrystals, decorating the surface of ∼10 nm TiO_2 nanoparticles. The surface of the larger TiO_2 nanoparticles (NPs) is partially covered by much smaller Cu NPs, attached to the surface of the larger NPs but not completely covering them due to the small quantity present (1–10 mol % Cu). This retards the anatase-to-rutile phase transition and titania domain growth through a grain-boundary pinning mechanism. These hybrid nanoparticles show tunable photochromic behavior under both UVA and visible light. Under UVA, Cu^{2+} nanoparticles reduce to Cu^{+}, and then to Cu^{0}. Under visible-light, Cu^{2+} reduces to Cu^{+}, although to a lesser extent. The induced photochromism can be tuned by varying the light source or exposure time. One mol % Cu causes a reduction of Cu^{2+}, and lowers the d–d absorption band, to 50% after only 12 s, and 95% after 10 min, under UVA-light, and has a reduction of 25% in 1 min, 50% in 4 min, and 80% in 1 h under visible-light. This is the first report of inorganic compounds, in this case Cu-TiO_2 hybrid nanoparticles, to exhibit tunable photochromism under both UVA and visible-light exposure. This rapid and sensitive effect can potentially be used to modify, tune, or monitor the progress of photoactivated behavior in a new generation of smart/active multifunctional materials and photoactive devices or sensors.

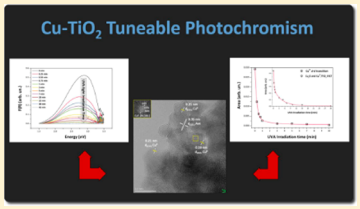

1. INTRODUCTION

The 21st century can be considered the "Nanotechnology Era" or "Nano-Age". As they possess unique physiochemical, catalytic, surface, and magnetic properties, nanomaterials may provide solutions to problems that cannot be dealt with using conventional technologies. As such, nanotechnologies are becoming an invaluable tool in many contexts. Among nanomaterials, metal oxides, because of their abundance and stability, play an increasingly dominant role. Among the oxides, the utilization of nano titanium dioxide (titania, TiO_2) is always growing, because of its wide range of applications, such as light-to-energy conversion and storage, and photocatalysis.[1−4]

Although TiO_2 is reported to have 11 bulk and/or nanocrystalline phases,[5] the three best known polymorphs of titania are rutile, anatase, and brookite, all of which are chemically inert, nontoxic, and also photocatalytically active (with no additives) in mild conditions. Anatase and rutile are employed in H_2 production,[6] are able to degrade both volatile organic compounds[7,8] and recalcitrant/persistent pollutants,[9] and are also reported to be active against several bacterial strains and yeasts.[10−12] TiO_2 has also been studied for its electrochromic behavior:[13,14] reversible and persistent changes in the optical properties can be obtained by charge insertion/extraction.[15]

Recently, TiO_2 has been shown to possess a degree of photochromic behavior; photochromism can be defined as that phenomenon in which the material can change color in a reversible way by exposure to an electromagnetic radiation (UV, visible, and IR illumination).[16] This phenomenon occurs when the surface of titania nanoparticles (NPs) are decorated with smaller noble metal NPs. When these noble-metal NPs (e.g., Ag, Au, Cu, and Pt) are embedded/decorated in/on a titania matrix and subjected to UV radiation, they can capture the photoexcited electrons from TiO_2 (due to photocatalysis) and become reduced to the metallic state.

This leads to a phenomenon known as multicolour photochromism,[17−19] because noble-metals NPs are able to absorb visible-light due to surface plasmon resonance (SPR).[20,21] This phenomenon occurs when the conducting electrons on the surface of the metallic NPs, exposed to a characteristic electromagnetic radiation, enter into a collective oscillation/excitation mode (a plasmon), induced by the electric field of the incident light.[22,23] The resonance is associated with a corresponding absorption of light:[24] in the case of gold, silver, and copper NPs, this SPR absorption falls into the visible range.[25]

In this work, copper has been chosen as a companion for titania, because of its ability to enhance both the visible-light absorption

Received: July 23, 2015
Revised: September 16, 2015
Published: September 16, 2015

DOI: 10.1021/acs.jpcc.5b07160
J. Phys. Chem. C 2015, 119, 23658–23668

and the photocatalytic activity (PCA) under UV-light exposure,[26] as well as because of its antimicrobial properties,[27,28] and its low cost compared to other noble-metals such as Au, Ag, or Pt.[29] Samples were synthesized via a "green" aqueous sol−gel nanosynthesis method,[30,31] and their phase composition and microstructure were thoroughly characterized, the former via the Rietveld method, the latter by way of a novel and advanced X-ray method, known as whole powder pattern modeling (WPPM). The optical properties (photochromic behavior) were fully addressed by means of diffuse reflectance spectroscopy (DRS). High resolution transmission electron microscopy (HR-TEM) was employed to detect any possible (re)formation of Cu NPs after UVA-light exposure.

This is the first, unprecedented report of inorganic NPs possessing tunable photochromic properties under both UVA and visible-light exposure. They could potentially be used for creating multifunctional smart or active coatings with applications in self-cleaning surfaces, photocatalysis, antimicrobial self-sterilizing materials, photoelectrochemical cells and sensors, and photochromism could be used to either modify or monitor in real time the progress of such photoactivated behavior in materials and devices.

2. EXPERIMENTAL SECTION

2.1. Sample Preparation. Aqueous titanium(IV)hydroxide sols were made via the carefully controlled hydrolysis and peptization of titanium(IV)isopropoxide (Ti-*i*-pr, $Ti(OCH(CH_3)_2)_4$) with distilled water diluted in isopropyl alcohol (IPA, propan-2-ol), following a protocol previously reported in detail by the authors.[30] In brief, one part of Ti-*i*-pr (Aldrich, 97%) was added to four parts of isopropyl alcohol to make a 20 vol % Ti-*i*-pr solution. This Ti-*i*-pr solution was hydrolyzed by the dropwise addition of an excess of water (5:1 water:Ti-*i*-pr) employed as a 20 vol % solution in IPA. The acid necessary to peptise the sol (concentrated HNO_3, Aldrich, 65%) was also added to this water−IPA solution, in a molar ratio of Ti^{4+}:acid of 2.5:1. This water−IPA-acid solution was added dropwise to the Ti-*i*-pr solution at room temperature, while being stirred. The precipitated mixture was evaporated to a white jelly like mass on a rotary evaporator, removing the IPA. Distilled water was added to restore the mixture to the original volume, and this was then dried once more to a dried gel at 60 °C. This gel could be redispersed in under 1 min to form a stable titania sol.

Four Cu-doped sols were prepared as well, with a $Cu:TiO_2$ molar ratio of 1, 2, 5, and 10 mol %. Stoichiometric amounts of copper(II) nitrate trihydrate (Aldrich, ≥ 98.5%) were added to the sol, which had a 1 M concentration. Afterward, dried gels were thermally treated at 450 °C under a static air flow, using a muffle furnace. The heating/cooling rate was 5 °C min^{-1}, with a 2 h dwell time at the selected temperature. Samples were referred to as **Ti450** (unmodified TiO_2), and **Cu−Ti450, 2Cu−Ti450, 5Cu−Ti450**, and **10Cu−Ti450** for 1 mol %, 2 mol %, 5 mol %, and 10 mol % of Cu addition, respectively.

2.2. Sample Characterization. A semiquantitative phase analysis (QPA) of the crystalline phases in the various specimens was obtained by X-ray powder diffraction (XRPD) using the Rietveld method as implemented in GSAS-EXPGUI.[32,33] Data were collected on a PANalytical X'Pert Pro (NL) θ/θ diffractometer equipped with 0.5° divergence slit, 0.5° antiscattering slit, 0.04 rad Soller slits, a 15 mm copper mask in the incident beam pathway and a fast RTMS detector (PIXcel 1D, PANalytical) on the diffracted arm. The 20−80°2θ range was investigated using Cu Kα radiation (45 kV and 40 mA) with a virtual step scan of 0.02°2θ and virtual time per step of 200 s. The starting atomic parameters for anatase, rutile and brookite, described in the space groups $I4_1/amd$, $P4_2/mnm$ and $Pbca$ respectively, were taken from the literature.[34,35] The instrumental contribution, evaluated by means of the NIST SRM 660b standard (LaB_6), was taken into account in the refinements. The refined parameters were: scale-factors, zero-point, specimen displacement, six coefficients of the Chebyshev background polynomial and unit cell parameters, two Lorentzian (L_X and L_Y) terms, and one angle independent Gaussian term (G_W) as the profile coefficients.

Whole powder pattern modeling (WPPM),[36] implemented in the PM2K software,[37] was employed for the microstructure analysis. This technique exploits XRPD as well, by describing each observed peak profile as a convolution of instrumental and sample-related physical effects, and refining the corresponding model parameters directly on the observed data.[38,39] Microstructure information such as crystalline domain shape, size distribution, defect type, and content can be quantitatively obtained. The results provided by the WPPM surpass those frequently obtained using integral breadth methods for line profile analysis (LPA), such as the Scherrer formula,[40] or the Williamson−Hall plot,[41] in terms of quality and quantity. Traditional LPA techniques are in fact based on simplified hypotheses (often not met), and the corresponding results are hard to interpret in terms of physical quantities that could be measured with alternative techniques (e.g., microscopy).[42]

Crystalline domains were assumed to be spherical and their diameter distributed according to a log-normal curve. On the grounds of HR-TEM observations (see below), anatase and rutile in **Ti450** were described using two models; the first considering a unimodal and the second a bimodal size distribution. [From a rigorous statistical point of view, we are not dealing with a bimodal distribution, as this definition would imply the presence of two absolute maxima in the probability distribution function. In our case the definition is more relaxed and we consider a distribution characterized by the presence of two maxima, independent of whether they are absolute or just local.] To improve the accuracy of the result, data with a high signal/noise ratio were employed, collected using the same

Table 1. Rietveld Agreement Factors and Crystalline Phase Composition of the Unmodified and Cu-Modified TiO_2[a]

		agreement factors			phase composition (wt %)		
sample	no. of variables	$R(F^2)$ (%)	R_{wp} (%)	χ^2	anatase	rutile	brookite
Ti450	27	2.30	4.15	1.37	55.6 ± 0.2	20.1 ± 0.2	24.3 ± 0.9
Cu−Ti450	20	3.16	3.60	2.03	82.2 ± 0.1	9.0 ± 0.2	8.8 ± 0.8
2Cu−Ti450	22	4.44	3.74	2.07	81.4 ± 0.1	8.8 ± 0.2	9.8 ± 0.8
5Cu−Ti450	21	3.36	3.01	1.76	84.9 ± 0.1	5.0 ± 0.2	10.1 ± 0.5
10Cu−Ti450	20	4.92	3.14	1.86	83.4 ± 0.1	4.2 ± 0.3	12.3 ± 0.5

[a]Note: there were 2285 observations for every refinement; the number of anatase, rutile, and brookite reflections was 32, 31, and 153, respectively.

DOI: 10.1021/acs.jpcc.5b07160
J. Phys. Chem. C 2015, 119, 23658−23668

instrument and setup described above, but in the 20−115°2θ range, with a virtual step of 0.1°2θ, and virtual time per step of 500 s. The instrumental contribution was obtained by parametrizing the profile of 14 reflections from the NIST SRM 660b standard (LaB_6), according to the Caglioti et al. relationship.[43] The following parameters were refined: background (6th-order Chebyshev polynomial), peak intensities, specimen displacement, lattice parameters, mean and variance of the size distributions, and screw and edge dislocation density.

To investigate their photochromic properties, samples (0.1 g) were exposed, for different irradiation times, to either UVA− or visible-light (cf. section 3.2). The lamps used for this purpose were a PL-S 9W (Philips, NL) germicidal lamp as UVA-light source and a PL-S 2P 9*W*/840 fluorescent lamp (Philips, NL), as visible-light source. The intensity of the radiation reaching the samples, measured with a radiometer (Delta OHM, HD2302.0, IT), was estimated to be ∼22 W m^{-2} in the UVA range (315 nm < λ < 400 nm), and ∼50 W m^{-2} in the visible region (λ > 400 nm, being nil in the UVA). Irradiation times are consecutive and absolute: a specimen irradiated for 0.25 min and then for a further 0.25 min will be identified as 0.50 min. Immediately after irradiation, diffuse reflectance spectroscopy (DRS) was performed using a Shimadzu UV 3100 (JP) spectrometer, equipped with a $BaSO_4$ integrating sphere. Spectra of the samples were acquired in the UV−vis range (250−825 nm) with 0.2 nm resolution with $BaSO_4$ as reference. To obtain a proxy for the absorption spectrum, we analyzed the DRS data with the Kubelka−Munk function:

$$\alpha \approx F(R_\infty) \equiv \frac{(1 - R_\infty)^2}{2R_\infty} = \frac{K}{S} \quad (1)$$

where K and S are, respectively, the absorption and scattering coefficients and $R_\infty = R_{sample}/R_{standard}$.[44]

The morphology of the samples was investigated with a 2200FS JP (JEOL) HR-TEM equipped with an energy dispersive X-ray spectroscopy (EDS) attachment (Oxford Instruments, UK), and with a Gatan Ultrascan 4000 SCCD camera. Fast Fourier transform (FFT) patterns were analyzed through the JEMS software package.[45] Samples were prepared by dispersing the NPs in IPA, and evaporating some drops of the suspension on carbon-coated copper TEM grids. In order to detect any (reformed) Cu NPs, a set of TEM specimens was also irradiated for 300 min with the UVA lamp prior to carrying out the analysis.

3. RESULTS AND DISCUSSION

3.1. X-ray Analysis. As an example, Figure S1 (electronic Supporting Information, ESI) shows the X-ray diffraction pattern of the **5Cu−Ti450** specimen and the corresponding Rietveld refinement: the QPA results are proposed in Table 1. The unmodified TiO_2, **Ti450**, contains 55.6 wt % anatase, 20.1 wt % rutile, and 24.3 wt % brookite. The sizable presence of this latter TiO_2 polymorph is to be attributed to the acidic condition of the synthesis,[30,46] that does not favor its conversion into rutile. Neither Cu^0, nor any Cu oxide (tenorite or cuprite) are detected in the XRD patterns of Cu-modified TiO_2, probably because the doping levels are too low, but also because the main reflections of Cu^0 and Cu oxides overlap those of anatase, rutile, and brookite.

Furthermore, the addition of Cu ions seems to delay considerably the anatase-to-rutile phase transition (ART), to the extent that all the Cu-modified titania contains >80 wt % anatase, *cf* Table 1. Moreover, the amount of rutile decreases with the amount of Cu doping in the system. Due to the greatly increased

Table 2. WPPM Agreement Factors and Unit Cell Parameters for the Three Phases in the Synthesised Samples

sample	agreement factors			unit cell parameters								
				anatase			rutile			brookite		
	R_{wp} (%)	R_{exp} (%)	χ^2	$a = b$ (nm)	c (nm)	V (nm^3)	$a = b$ (nm)	c (nm)	V (nm^3)	a (nm)	b (nm)	c (nm)	V (nm^3)
Ti450	6.17	1.96	3.15	0.3791(1)	0.9515(1)	0.137(1)	0.4598(1)	0.2959(1)	0.063(1)	0.5440(2)	0.9206(4)	0.5157(1)	0.258(1)
Cu−Ti450	2.53	2.09	1.21	0.3790(1)	0.9510(3)	0.137(1)	0.4600(1)	0.2959(1)	0.063(1)	0.5459(4)	0.9129(29)	0.5147(7)	0.256(2)
2Cu−Ti450	3.85	1.95	1.97	0.3790(1)	0.9511(3)	0.137(1)	0.4600(1)	0.2961(1)	0.063(1)	0.5455(6)	0.9105(37)	0.5144(6)	0.255(2)
5Cu−Ti450	2.72	1.88	1.44	0.3791(1)	0.9510(4)	0.137(1)	0.4603(1)	0.2962(1)	0.063(1)	0.5454(7)	0.9108(73)	0.5143(8)	0.255(3)
10Cu−Ti450	3.16	1.71	1.84	0.3796(2)	0.9507(6)	0.137(1)	0.4604(2)	0.2963(2)	0.063(1)	0.5462(7)	0.9120(52)	0.5142(8)	0.256(2)

DOI: 10.1021/acs.jpcc.5b07160
J. Phys. Chem. C 2015, 119, 23658−23668

Table 3. Mean Crystalline Domain Size of Anatase (ant), Rutile (rt), and Brookite (brk), Defined As the Mean of the Lognormal Size Distribution; Mode of the Lognormal Size Distribution

	mean crystalline domain diameter			mode of the size distribution		
sample	$\langle D_{ant}\rangle$ (nm)	$\langle D_{rt}\rangle$ (nm)	$\langle D_{brk}\rangle$ (nm)	Ant (nm)	Rt (nm)	Brk (nm)
Ti450	10.4 ± 0.7	14.4 ± 0.6	7.0 ± 0.1	9.4 ± 0.6	9.9 ± 0.4	5.3 ± 0.1
Cu−Ti450	8.0 ± 0.2	12.2 ± 1.1	4.3 ± 0.5	6.6 ± 0.2	8.6 ± 0.8	3.8 ± 0.4
2Cu−Ti450	8.8 ± 0.2	10.3 ± 1.0	4.1 ± 0.3	7.9 ± 0.2	6.8 ± 0.6	3.8 ± 0.3
5Cu−Ti450	7.4 ± 0.2	7.7 ± 0.9	3.9 ± 0.7	6.4 ± 0.2	5.4 ± 0.7	3.6 ± 0.7
10Cu−Ti450	6.3 ± 0.3	9.2 ± 1.4	4.1 ± 0.4	5.3 ± 0.3	7.1 ± 1.1	3.8 ± 0.4

Table 4. WPPM Agreement Factors, Unit Cell Volume (V) and Average Domain Diameter of the Two Fractions of Anatase and Rutile According to the Proposed Bimodal Size Distribution Model

	agreement factors			anatase_1		anatase_2		rutile_1		rutile_2	
sample	R_{wp} (%)	R_{exp} (%)	χ^2	V (nm^3)	average size (nm)	V (nm^3)	average size (nm)	V (nm^3)	average size (nm)	V (nm^3)	average size (nm)
Ti450	3.94	1.86	2.11	0.137(1)	11.3 ± 0.1	0.135(1)	32.4 ± 0.1	0.062(1)	10.7 ± 0.2	0.063(1)	27.2 ± 4.2
Cu−Ti450	2.62	1.99	1.31	0.136(1)	7.9 ± 0.6	0.137(1)	16.8 ± 2.6	0.063(1)	11.0 ± 1.8	0.063(1)	16.7 ± 8.6
2Cu−Ti450	2.43	1.98	1.23	0.137(1)	8.6 ± 0.3	0.137(1)	15.8 ± 1.0	0.063(1)	9.9 ± 1.2	0.062(1)	18.5 ± 0.4
5Cu−Ti450	2.18	1.80	1.21	0.137(1)	7.0 ± 0.4	0.137(1)	20.3 ± 0.7	0.063(1)	12.3 ± 0.1	0.062(1)	16.9 ± 0.2
10Cu−Ti450	2.05	1.72	1.19	0.137(1)	6.1 ± 0.2	0.137(1)	24.9 ± 4.8	0.063(1)	8.4 ± 2.4	0.062(1)	16.1 ± 0.1

amount of anatase present, the content of brookite is clearly lower in all the Cu-modified samples (amounts ranging from 8.8 wt % in **Cu−Ti450**, to 12.3 wt % in **10Cu−Ti450**). Nevertheless, it is worth noting that the amount of brookite in Cu-modified samples increases with Cu mol %, at the expense of rutile (Table 1), indicating that Cu addition also delays the brookite → rutile phase transformation.

This delay of the ART is in contrast with the common belief that Cu accelerates it. For some authors, this accelerating behavior is due to electron pumping from copper directly into the TiO_2 conduction band;[47,48] other authors invoke the effect of excess oxygen vacancies to explain the same phenomenon.[49−51] We claim that Cu doping, as done here, actually causes a grain-boundary pinning,[52,53] resulting in delaying the ART as a consequence of a nucleation−growth mechanism.[47]

WPPM data are reported in Tables 2−4, and in Figure 1a−c; in Figure S2a,b are depicted examples of the WPPM output. Observing the negligible differences in unit cell volumes (Table 2), we can see that Cu did not significantly enter into the structure of anatase, rutile and brookite, given the ionic radii of $^{[VI]}Cu^{1+/2+}$ = 0.77/0.73 Å and of $^{[VI]}Ti^{4+}$ = 0.61 Å.[54] On the other hand, the change in the tetragonality of anatase, the a/c ratio, increases very slightly with the copper content (i.e., an increase of 0.24% in anatase), which might suggest the presence of some local lattice distortion.

The large line profile broadening suggests that all three phases are nanocrystalline. Considering them as monodispersed, we can see in Table 3 that in **Ti450**, rutile domains have an average of 14.4 nm, and the other two polymorphs have averages of 10.4 nm (anatase) and 7.0 nm (brookite). Increasing the copper amount, the size distribution becomes narrower, cf. Figure 1a−c. Copper addition also causes the reduction of the average anatase domain size (cf. Table 3, and Figure 1a): the greater the amount of Cu, the greater the reduction in size, with anatase in **10Cu−Ti450** being roughly 2/3 of the size of that in unmodified **Ti450**. Rutile preserves a wider size distribution (cf. Figure 1b, and Table 3), but the average still decreases by around 1/3. In brookite, copper causes the greatest decrease in the average domain diameter−being in the 4 nm range vs 7 nm in the unmodified TiO_2, Figure 1c−and also a greater narrowing of the size distribution. Metallic copper NPs presumably nucleate on the grain boundaries, pinning them, thus limiting their further growth, explaining the delay of the ART.

The WPPM result for sample **Ti450** based on the monodispersed model (*cf* Figure S2a) does not lead to a perfect fit, as some features are still present in the difference curve. Suspecting that the phenomenon might be attributed to a nonideal distribution of the domain sizes, we collected some HR-TEM evidence−the micrograph of **Ti450**, Figure 2, clearly shows the simultaneous presence of large and small domains. The WPPM analysis was performed a second time considering a bimodal size distribution for anatase and rutile (a monodispersed distribution was sufficient to model the brookite fraction).

Synthetic WPPM results for this bimodal size distribution model are shown in Table 4, and Figure S3a,b. The introduction of a second fraction does not change the unit cell parameter results (sizes and volume are unaltered). As for the domain size, we see the appearance of a large-size fraction of rutile (16.1−27.2 nm, coexisting with domains of 8.4−12.3 nm), and a large-size fraction of anatase (15.8−32.4 nm coexisting with 6.1−11.2 nm). The extra fraction of material accounts for the presence of a long tail in the actual distribution directed toward lower sizes for rutile and higher sizes for anatase. The fact that the monodisperse model captures just one or the other value is related to the physics of diffraction, sensitive to volume and therefore to the fraction that, in volume, is the dominant one. This offers the possibility to appreciate the sensitivity of modern line profile analysis techniques, as the addition of this small quantity is sufficient to improve the quality of the modeling (cf. Figure S2a,b).

3.2. DRS Analysis: Photochromism. *3.2.1. UVA-Light Exposure.* Diffuse reflectance spectra of **Ti450**, and Cu-TiO_2 samples prior to UVA irradiation are shown in Figure 3. Sample **Ti450** shows one absorption band, at around 400 nm, due to the $Ti^{4+}−O^{2−}$ metal−ligand charge transfer (MLCT);[55] this feature is also present in the Cu-modified samples. Furthermore, Cu-modified samples also display absorption features in the visible region, related to electronic transitions involving copper ions. In **Cu−Ti450**, the absorption at around 450 nm is attributed to the electron transfer from the valence band of TiO_2

DOI: 10.1021/acs.jpcc.5b07160
J. Phys. Chem. C 2015, 119, 23658−23668

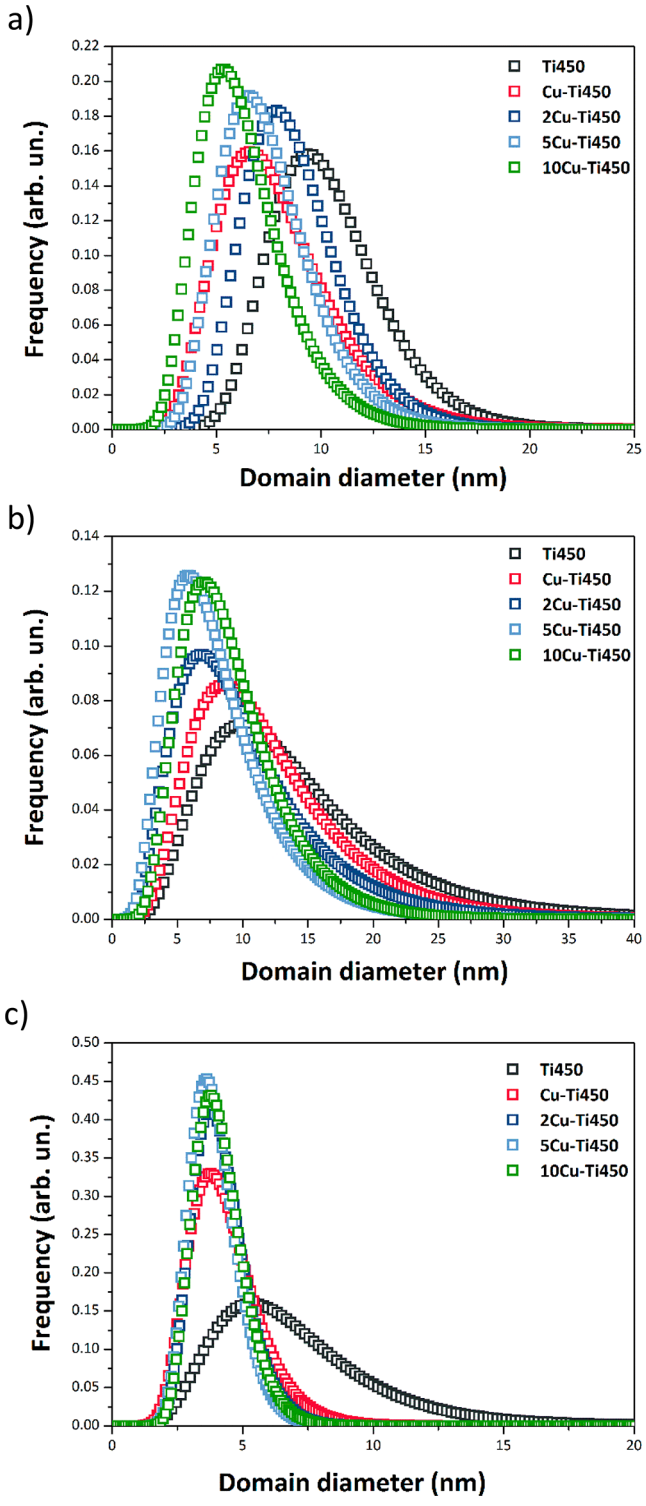

Figure 1. Unimodal size distribution of (a) anatase, (b) rutile, and (c) brookite, as obtained from the WPPM analysis.

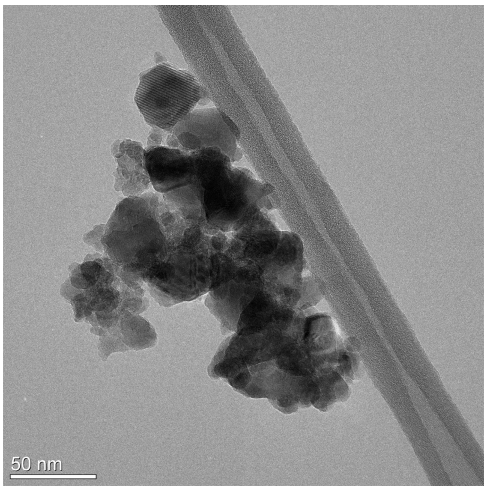

Figure 2. HR-TEM micrograph of sample **Ti450** showing the coexistence of large and small TiO_2 crystalline domains.

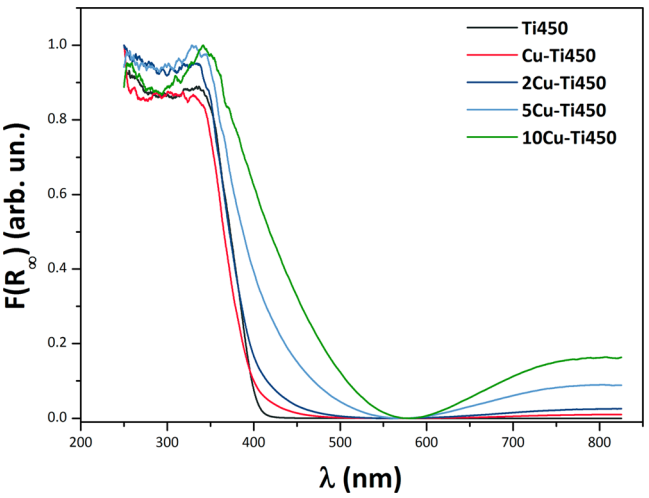

Figure 3. DRS spectra of prepared samples, prior to UVA- visible-light exposures.

to that of Cu_xO clusters that are around titania (intervalence charge transfer, IVCT).[56] The IVCT effects increase with the increasing amount of Cu (cf. samples **2Cu−Ti450**, **5Cu−Ti450**, and **10Cu−Ti450**). In the samples with Cu > 1 mol %, the absorption tail extends, up to 575 nm in **10Cu−Ti450**: this is commonly ascribed to interband absorptions in Cu_2O.[57,58] The presence of Cu_xO clusters around titania is also seen in HR-TEM micrographs, Figure 4a,b. Even prior to UV exposure, some Cu^0 nanocrystals are observed, as the copper reduction is very fast, and even exposing the samples to day-light for a few seconds during TEM sample preparation and transportation has an effect, resulting in some metallic Cu nanocrystals. Moreover, also the electron beam of TEM is able to reduce, to a certain degree, copper to its Cu metallic form. Furthermore, Cu^{2+} being a strong absorber, the absorption band seen above 600 nm, and centered at around 800 nm (producing the green hue of the sample), is assigned to its d−d electronic transition.[55,56,59,60] The intensity of that band increases with the amount of Cu^{2+} present in the samples.

DRS was likewise used to study the photochromism of Cu-modified TiO_2 samples. In general, when a Cu-modified sample is exposed to UVA light for increasing time, changes occur to the spectrum. As an example, Figure 5 reports the behavior of **Cu−Ti450** irradiated with UVA light for up to 1 min. Under irradiation, the valence electrons of TiO_2 are pushed into the conduction band, leaving a hole behind.[61] These excited electrons can migrate to the valence band of the Cu_xO clusters (thus enhancing the absorption tail centered at ∼450 nm), and are also able to reduce the Cu^{2+} ions, to create−or enhance, where already present−the absorption tail in the 500−600 nm range (due to Cu_2O). As a consequence of this Cu^{2+} reduction,

DOI: 10.1021/acs.jpcc.5b07160
J. Phys. Chem. C 2015, 119, 23658−23668

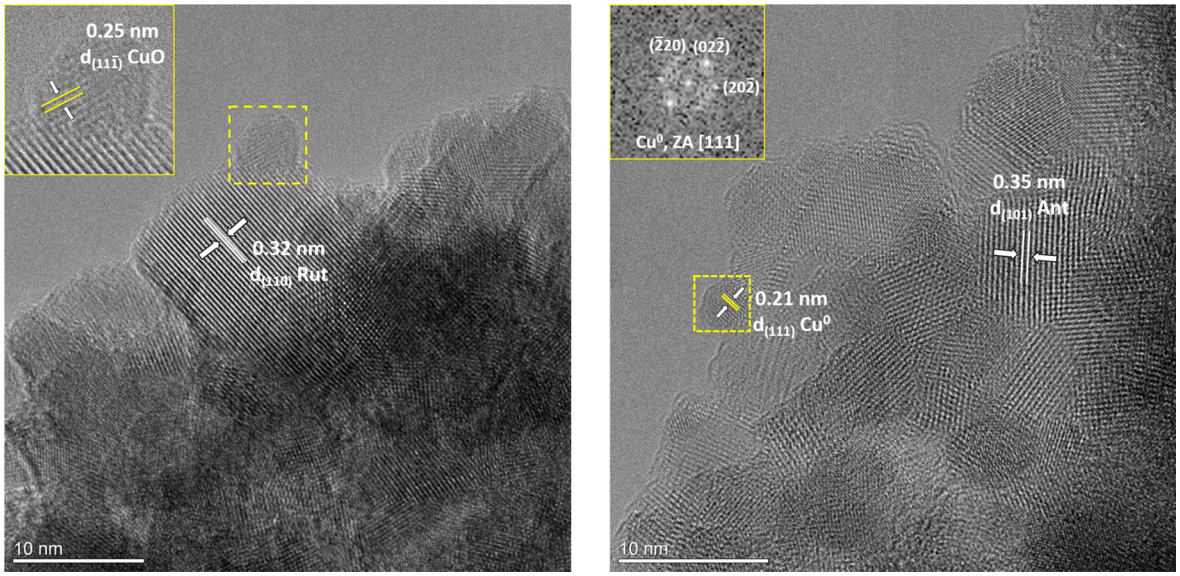

Figure 4. HR-TEM micrographs of: (a) sample **5Cu−Ti450**: a CuO NP (yellow-dashed square), is visible—a magnification of it being depicted in the inset—is clustered around a bigger NP of rutile; their $d(11\bar{1})$ and $d(110)$ crystallographic planes are shown, respectively. (b) Sample **10Cu−Ti450**: a Cu^0 NP is highlighted, and the inset displays its FFT pattern (obtained from yellow-dashed square area), described in the zone axis (ZA) [111]. Also, the $d(101)$ crystallographic planes of a NP of anatase are shown.

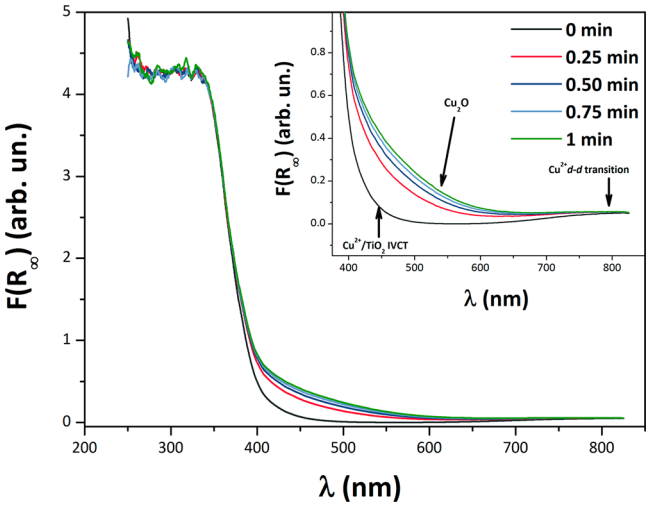

Figure 5. DRS spectra of sample **Cu−Ti450** irradiated with UVA-light for 0, 0.25, 0.50, 0.75, and 1 min. The inset shows the λ range 375−850 nm, highlighting the progressive disappearance of the absorption band due to Cu^{2+} d−d transition.

the absorption band due to Cu^{2+} d−d electronic transition gradually decreases (Figure 5, and its inset).

In order to quantitatively examine the evolution of the specimens, the absorption band due to the Cu^{2+} d−d electronic transition was modeled with a Gaussian function (OriginPro, version 8.5.0), and the full width at half-maximum (fwhm, band splitting), the area of the peak (optical density), and its centroid (energy),[62] were extracted (see Tables 5 and 6). The absorption bands due to the reduced Cu_2O (at around 500−600 nm), and that due to Cu^{2+}/TiO_2 IVCT (at ∼450 nm) were also monitored. In the latter case, a spectrum taken at a certain irradiation time, depending on the sample, was taken as a baseline, and subtracted from all others (Figure 6). Afterward, the same parameters (i.e., fwhm, peak area and centroid) were extracted (cf. Tables 5 and 6, columns 5−7). It can be seen in Figure 6 that for **Cu−Ti450**, there is a large decrease in the Cu^{2+} d-d transition in a very short time, with a reduction of ∼50% after just 12 s of UVA-light irradiation, and a reduction of >95% after 10 min. This signifies that this effect could be monitored to give detailed and precise information on exposure times, or that small exposure times have a large effect on the tuning of these values.

The spectroscopic data of **Cu−Ti450** are reported in Table 5. We can obtain quantitative information about the reduction of copper by noting that the optical density is proportional to the population of Cu^{2+} ions in the sample.[63] Plotting the optical density vs the UVA irradiation time (Figure 7) and assuming in this case that, at time zero, copper is only present as the cupric ion (Cu^{2+}), we can observe an almost exponential decrease in the Cu^{2+} population. An analogous plot can be made for the other transition (Cu_2O and Cu^{2+}/TiO_2 IVCT), as reported in the inset of Figure 7, which also represents the ongoing reduction of $Cu^+ \rightarrow Cu^0$.

The observation of Figure 7 can be interpreted by assuming that the number of Cu^{2+} ion-reduction events, dy in a given interval of time dt is proportional to the number y of ions still present (A is the proportionality constant). The solution of the resulting differential equation $\partial y/\partial t = -At$ is an exponential decay law $y = Ae^{-t/\tau}$. A constant can be added to the equation to consider the possible inaccuracy due to the choice of the limiting state in extracting the population information. Modeling with a single exponential decay, however, is not satisfactory. In fact, in all the studied cases (i.e., using both light sources and monitoring the three absorption bands), a better fit is obtained by adopting a shifted double exponential decay function ($y = y_0 + A_1e^{-t/\tau_1} + A_2e^{-t/\tau_2}$). This suggests the simultaneous occurrence of (at least) two distinct processes in the reduction of the Cu^{2+} d−d absorption band, and in that of Cu_2O and Cu^{2+}/TiO_2 IVCT. The fit is good (cf. Figure 7, and its inset): Cu^{2+} is quickly reduced to half of its starting amount in approximately 0.20 min (only 12 s). Thus, very short UVA-light exposures are able to start the reduction of Cu^{2+}, and at the same time, can promote a charge transfer from the valence band of TiO_2 to that of the Cu_xO NPs clustered around titania. We can, in fact clearly see the Cu^{2+}/TiO_2 IVCT appearing together with a reduction of the

DOI: 10.1021/acs.jpcc.5b07160
J. Phys. Chem. C 2015, 119, 23658−23668

Table 5. Energy (Centroid), Band Splitting (FWHM), and Intensity (Area) of the Cu^{2+} d−d Transition and Cu_2O and Cu^{2+}/TiO_2 IVCT Transitions in Cu−Ti450 after UVA-Light Irradiation Time[a]

	Cu^{2+} d−d transition			Cu_2O and Cu^{2+}/TiO_2 IVCT		
UVA-light exposure time (min)	centroid (eV)	FWHM (eV)	area (arb. units)	centroid (eV)	FWHM (eV)	area (arb. units)
0	1.5125(5)	0.5388(11)	0.0293(1)	2.7930(11)	0.9946(39)	0.5418(27)
0.25	1.5403(12)	0.4727(46)	0.0124(2)	2.7218(7)	1.1002(28)	0.3587(13)
0.50	1.5572(16)	0.4043(63)	0.0061(2)	2.7107(6)	1.1452(27)	0.2957(10)
0.75	1.5921(14)	0.3852(107)	0.0045(3)	2.7016(6)	1.1665(27)	0.2559(9)
1	1.6040(12)	0.3345(97)	0.0025(1)	2.6791(9)	1.1356(41)	0.2150(12)
3	1.7078(21)	0.2680(185)	0.0011(2)	2.6484(12)	1.1274(57)	0.1315(10)
5	1.7354(19)	0.2206(61)	0.0011(1)	2.6475(7)	1.1810(32)	0.1030(4)
7	1.7177(58)	0.1792(135)	0.0008(1)	1.6047(34)	0.8697(78)	0.0493(6)
10	1.7561(34)	0.1095(82)	0.0003(1)	1.6098(44)	0.7740(101)	0.0255(4)
15				2.5353(11)	1.1352(62)	0.0239(2)
30				2.4361(13)	1.1789(116)	0.0059(1)

[a]The coefficient of determination R^2 was ≥0.902 for all the fitting of the *d-d* transition. For the IVCT, R^2 was ≥0.954 for all the data.

Table 6. Energy (Centroid), Band Splitting (FWHM), and Intensity (area) of the Cu^{2+} d−d Transition and Cu_2O and Cu^{2+}/TiO_2 IVCT Transitions in Cu−Ti450 after Visible-Light Irradiation Time[a]

	Cu^{2+} d−d transition			Cu_2O and Cu^{2+}/TiO_2 IVCT		
visible-light exposure tim (min)	centroid (eV)	FWHM (eV)	area (arb. units)	centroid (eV)	FWHM (eV)	area (arb. units)
0	1.5090(8)	0.5206(25)	0.0180(1)	2.8532(11)	0.9804(33)	0.3506(14)
0.25	1.5153(6)	0.5151(14)	0.0165(1)	2.8299(10)	1.0087(32)	0.3211(12)
0.50	1.5197(6)	0.5006(15)	0.0147(1)	2.8260(9)	1.0264(28)	0.3081(10)
0.75	1.5262(8)	0.4850(17)	0.0144(1)	2.8060(10)	1.0201(33)	0.2888(12)
1	1.5285(6)	0.4757(14)	0.0127(1)	2.8021(10)	1.0096(34)	0.2759(12)
3	1.5315(9)	0.4653(25)	0.0105(1)	2.7862(10)	1.0308(36)	0.2362(10)
5	1.5428(8)	0.4267(23)	0.0083(1)	2.7754(10)	1.0456(37)	0.2110(10)
7	1.5447(10)	0.4096(31)	0.0073(1)	2.7513(12)	1.0350(45)	0.1835(10)
10	1.5529(9)	0.4100(38)	0.0065(1)	2.7618(11)	1.0648(39)	0.1718(8)
15	1.5541(11)	0.3899(46)	0.0049(1)	2.7802(8)	1.1208(31)	0.1580(6)
30	1.5631(9)	0.3685(51)	0.0035(1)	2.7752(14)	1.2453(313)	0.1465(87)
45	1.5833(12)	0.3252(85)	0.0026(1)	2.8062(11)	1.3048(522)	0.1244(129)
60	1.5917(12)	0.2701(57)	0.0015(1)	2.8210(11)	1.2891(404)	0.1178(94)
90	1.6019(8)	0.2302(41)	0.0008(1)	2.8035(14)	1.5196(499)	0.1154(96)
120	1.6171(12)	0.2174(13)	0.0005(1)	2.8182(15)	1.6860(2184)	0.1055(382)

[a]The coefficient of determination R^2 was ≥0.961 for all the fitting of the *d-d* transition, except for the fit at 120 min where R^2 = 0.873. For the IVCT, R^2 was ≥0.942 for all data.

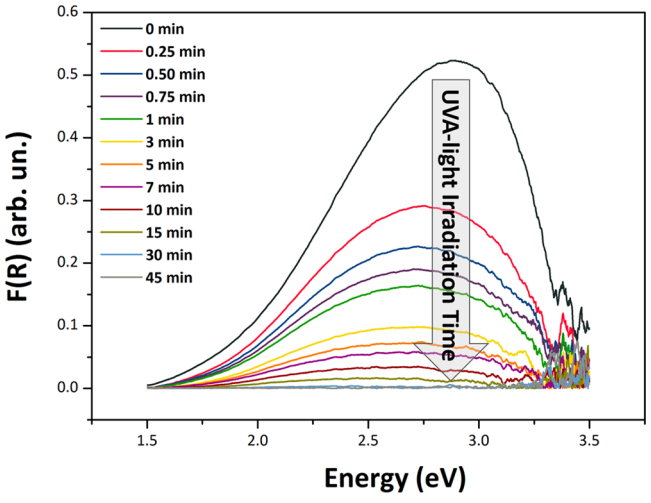

Figure 6. Spectra of the bands due to the reduced Cu_2O, and those due to Cu^{2+}/TiO_2 IVCT (intervalence charge transfer) under UVA-light, using the spectrum taken at 60 min UVA-light irradiation time as baseline−sample **Cu−Ti450**.

band due to the Cu^{2+} d−d electronic transition. By increasing the exposure time, both the optical density and band splitting of this transition decrease, indicating a progressive (and complete) reduction of Cu^{2+} (see Table 5). After 3 consecutive minutes of UVA irradiation, the signature of the Cu^{2+} d−d electronic transition almost disappears, and the specimen reverts from greenish to brownish (Figure S4a-b). Only the interband absorptions of Cu_2O and the MLCT of titania survive. Considering the area of the bands belonging to Cu_2O and Cu^{2+}/TiO_2 IVCT (Table 5 and inset of Figure 7), we can still see an exponential trend, and the process is therefore modeled following the same idea. However, this process seems slower, as the time needed to (ideally) reach the 50% decay is equal to 0.59 min (36 s).

With 2 mol % copper, **2Cu−Ti450**, spectroscopic data relative to UVA-light exposure are shown in Figure 8 and Table S1. It is clear that with 2 mol % Cu the picture becomes more complicated, as the spectra present features due to interband absorption of Cu_2O, which is equivalent to saying that the assumption that copper, at time zero, is only present as Cu^{2+}, is no longer valid. A higher copper amount in the sample leads to a slightly slower reduction of Cu^{2+}, as the area of the band due to Cu^{2+} d−d transition reduces to the half of its starting amount in

DOI: 10.1021/acs.jpcc.5b07160
J. Phys. Chem. C 2015, 119, 23658−23668

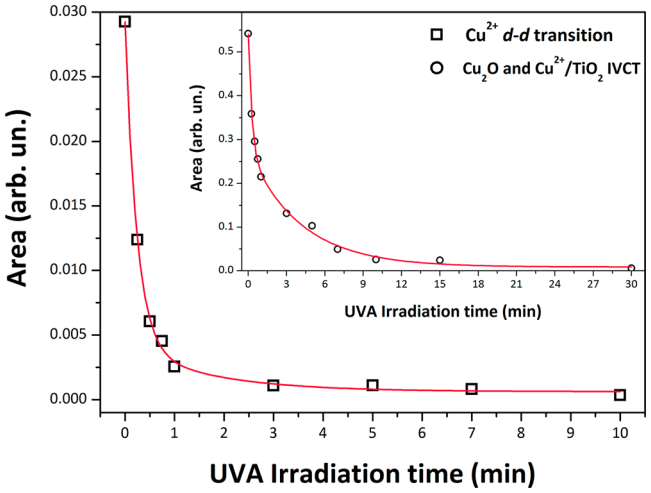

Figure 7. Area of the band due to the Cu^{2+} d−d transition in **Cu−Ti450** versus UVA exposure time (empty squares); the coefficient of determination R^2 of the double exponential decay function adopted for the fitting was 0.998. In the inset is reported area of the bands due to Cu_2O and Cu^{2+}/TiO_2 IVCT **Cu−Ti450** versus UVA exposure time (empty circles), the coefficient of determination R^2 was 0.996.

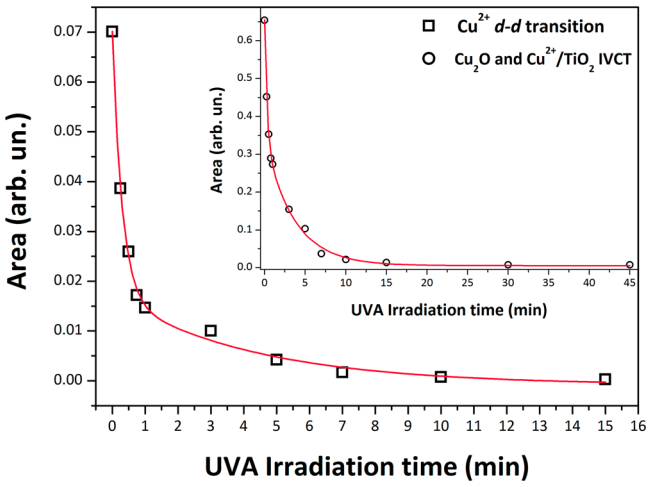

Figure 8. Area of the band due to the Cu^{2+} d−d transition in **2Cu−Ti450** versus UVA exposure time (empty squares); the coefficient of determination R^2 of the double exponential decay function adopted for the fitting was 0.997. In the inset is reported area of the bands due to Cu_2O and Cu^{2+}/TiO_2 IVCT **2Cu−Ti450** versus UVA exposure time (empty circles), the coefficient of determination R^2 was 0.998.

approximately 0.30 min (18 s, see Table 6 and Figure 8). For the Cu_2O and Cu^{2+}/TiO_2 IVCT bands, the time needed to reach 50% decay was roughly equal to 0.65 min (vs 0.59 min of **Cu−Ti450**), as shown in the inset of Figure 8. Furthermore, looking at the HR-TEM micrograph of this sample, taken after 300 min exposure under UVA-light (Figure 9), small ∼2 nm (re)formed Cu^0 NPs are clearly visible on the larger titania ones.

Increasing copper loading to 5 mol % (**5Cu−Ti450**), Table S2, we observe a further different behavior under UVA-light irradiation (Figure 10). The light is no longer able to reduce all the Cu^{2+} in the sample. It can be seen in Figure 10 that the area of the band due to the d−d electronic transition does not reach a plateau at zero, but levels out at ∼83% reduction. Also, the time needed to reach that plateau is longer, as it is reached after 90 min UVA irradiation time. Furthermore, also in this case, the best fit was obtained adopting a double exponential decay function, and

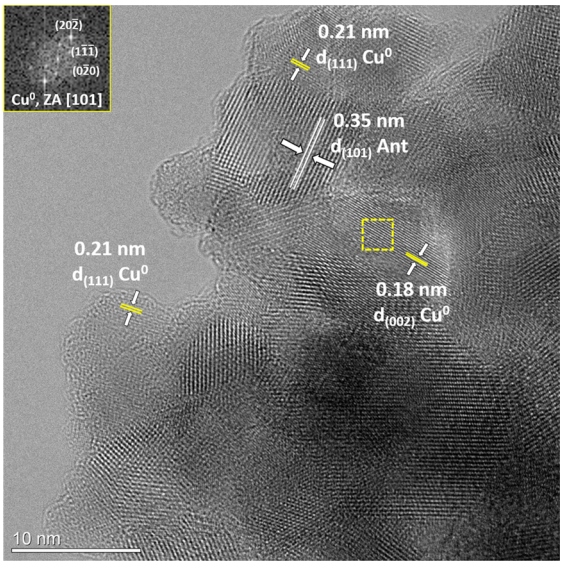

Figure 9. HR-TEM micrograph of sample **2Cu−Ti450** after 300 min of UVA-light irradiation time: reformed Cu^0 NPs are seen among larger titania ones (anatase $d_{(101)}$ crystallographic planes are shown). In the inset is reported the FFT pattern of a Cu^0 NP taken from the yellow-dashed square area, described in the ZA [101].

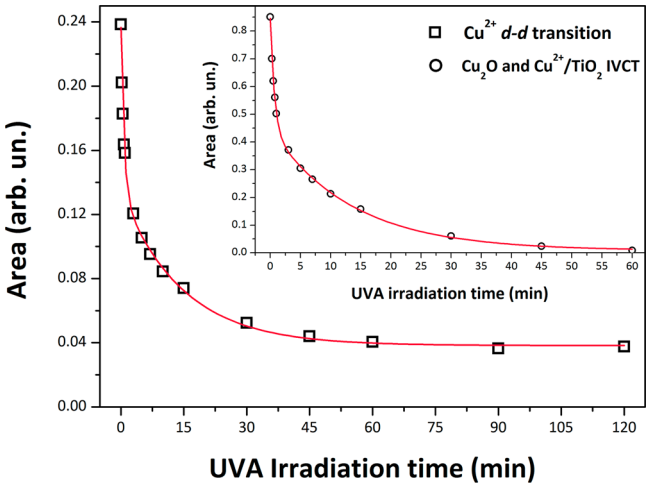

Figure 10. Area of the band due to the Cu^{2+} d−d transition in **5Cu−Ti450** versus UVA exposure time (empty squares); the coefficient of determination R^2 of the double exponential decay function adopted for the fitting was 0.998. In the inset is reported area of the bands due to Cu_2O and Cu^{2+}/TiO_2 IVCT **5Cu−Ti450** versus UVA exposure time (empty circles), the coefficient of determination R^2 was 0.999.

the time needed to reach the 50% decay increased to 2.95 min. On the contrary, monitoring the bands belonging to Cu_2O and Cu^{2+}/TiO_2 IVCT, the time needed to reach 50% decay is equal to 1.73 min, faster than that required to reduce 50% of the Cu^{2+} (inset of Figure 10).

With 10 mol % Cu (**10Cu−Ti450**), Table S3, the time needed to reduce 50% of the Cu^{2+} d−d electronic transition is greatly extended to 24.48 min, Figure 11, and its inset. This was, as in **5Cu−Ti450**, much longer than the time necessary to reduce to 50% the bands belonging to Cu_2O and to Cu^{2+}/TiO_2 IVCT, which is 2.48 min (cf. inset of Figure 11). The reduction of Cu^{2+} reaches a plateau at ∼62%. Hence, with Cu > 2 mol %, the reduction of Cu_2O and Cu^{2+}/TiO_2 IVCT becomes much faster than that of Cu^{2+}, and the reduction of Cu^{2+} is never complete.

DOI: 10.1021/acs.jpcc.5b07160
J. Phys. Chem. C 2015, 119, 23658−23668

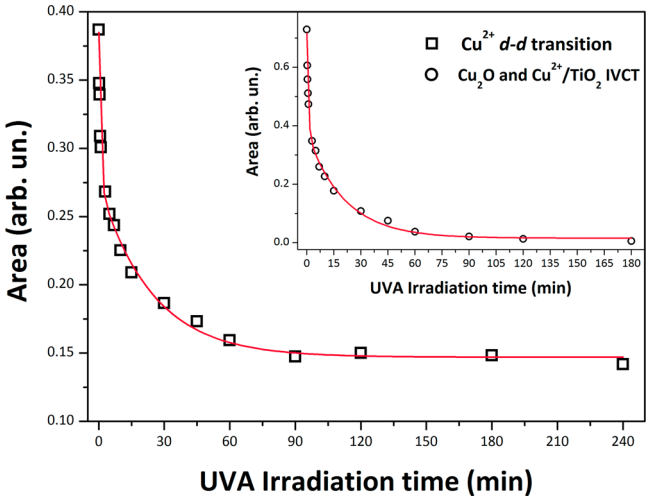

Figure 11. Area of the band due to the Cu^{2+} d−d transition in **10Cu−Ti450** versus UVA exposure time (empty squares); the coefficient of determination R^2 of the double exponential decay function adopted for the fitting was 0.995. In the inset is reported area of the bands due to Cu_2O and Cu^{2+}/TiO_2 IVCT **10Cu−Ti450** versus UVA exposure time (empty circles), the coefficient of determination R^2 was 0.997.

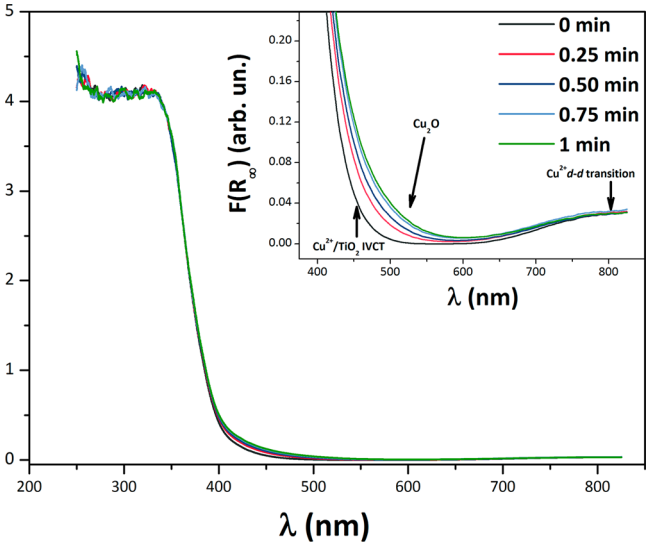

Figure 12. DRS spectra of sample **Cu−Ti450** irradiated with visible-light for 0, 0.25, 0.50, 0.75, and 1 min. The inset shows the λ range 375−850 nm, highlighting the progressive appearance and strengthening of Cu^{2+}/TiO_2 IVCT and interband absorptions in Cu_2O, together with the very weak disappearance of the absorption band due to Cu^{2+} d−d transition.

3.2.2. Visible-Light Exposure. Under visible-light exposure (Figure 12, and Table 6), we observe a similar behavior−hence the discussion here will be less detailed. However, this clearly shows that also under visible-light irradiation, there is an electron−hole separation (in other words, the photocatalytic mechanism), due to the presence of rutile in the samples. Rutile is actually reported to be a visible-light activated photocatalyst.[30] This also makes our material a potential photocatalyst for indoor applications. However, visible light was unable to reduce Cu^{2+} as strongly as that observed under UVA-light, especially for copper amounts >2 mol %; on the other hand, the light intensity in the visible range was strong enough to−at least−reduce to 50% the transitions due to Cu_2O and Cu^{2+}/TiO_2 IVCT.

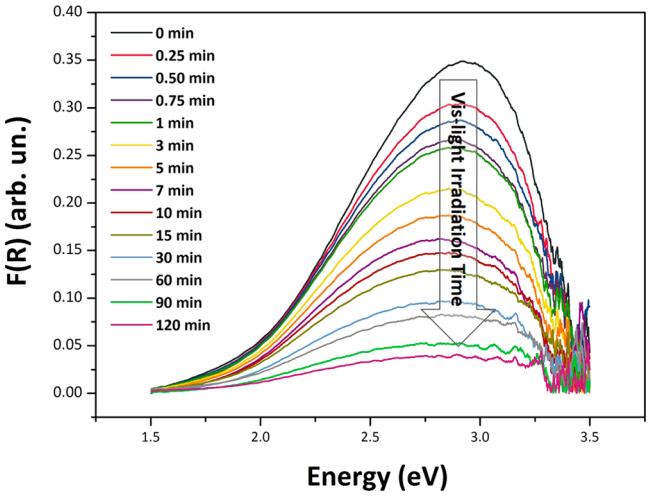

Figure 13. Spectra of the bands due to the reduced Cu_2O, and those due to Cu^{2+}/TiO_2 IVCT, under visible-light, using the spectrum taken at 180 min visible-light irradiation time as a baseline for sample **Cu−Ti450**.

With 1 mol % Cu (**Cu−Ti450**), Table 6, the time necessary to reduce the Cu^{2+} population to half is approximately equal to 3.74 min (vs 12 s using UVA-light); on the other hand, to reduce the Cu_2O and Cu^{2+}/TiO_2 IVCT transitions to their half, the time needed was 10.84 min (versus 36 s when using UVA-light), cf. Figure S5 and its inset. It can be seen in Figure 13, taken using exposure of **Cu−Ti450** to visible light for 180 min as a baseline, that even with visible light there is a large and relatively rapid decrease in the Cu^{2+} d−d transition, with a reduction of ∼25% after just 1 min of visible light irradiation, a reduction of ∼50% after 4 min and ∼80% after 1 h. This signifies that even under visible light, this effect could be used to sensitively monitor or tune the process.

With double the amount of copper (**2Cu−Ti450**, Table S4), the time to reduce the Cu^{2+} population to 50% was raised to 5.11 min, and 8.66 min was needed to halve the Cu_2O and Cu^{2+}/TiO_2 IVCT transitions (Figure S6, and its inset). With 5 mol % copper (**5Cu−Ti450**, Table S5 and Figure S7), 116.33 min were needed to halve the Cu^{2+} concentration, while to do the same to the Cu_2O and Cu^{2+}/TiO_2 IVCT transitions required 13.85 min. Finally, with 10 mol % Cu (**10Cu−Ti450**), cf. Figure S8, and Table S6, the light intensity in the visible region was not able to halve the initial Cu^{2+} amount, even after 300 min irradiation time; on the contrary, the transitions due to Cu_2O and Cu^{2+}/TiO_2 IVCT were halved in 20.14 min.

The induced photochromism can be therefore tuned by simply modifying the light source, the exposure time and the Cu concentration, under UVA or visible light, and is a sensitive and rapid process in both cases with 1 mol % Cu added.

Furthermore, as the photochromic behavior is reported to be reversible at room temperature,[64] a future prospect will be investigating the possible thermally assisted photochromic recovery behavior of such material when subjected to a mild thermal treatment.

4. CONCLUSIONS

Copper (0, 1, 2, 5, and 10 mol %) modified TiO_2 was made via a green synthesis method, based upon an environmentally friendly aqueous sol−gel technique. The effect of Cu addition on the anatase-to-rutile (ART) phase transition, and on the microstructure of the prepared samples was examined via advanced

DOI: 10.1021/acs.jpcc.5b07160
J. Phys. Chem. C 2015, 119, 23658−23668

X-ray methods. A bimodal size distribution model for anatase and rutile was proposed. It was found that Cu did not enter the TiO_2 lattice, and did not enhance the ART (commonly reported as a nucleation and growth mechanism), because of a grain-boundary pinning mechanism, that also retarded titania crystalline domain growth.

The photochromic behavior was also assessed in detail using UV−vis spectroscopy. It was found that under UVA-exposure, Cu^{2+} reduced to Cu^{+} and then to Cu^{0} NPs. Under visible-light exposure, Cu^{2+} was reduced to Cu^{+}, although to a lesser extent. The induced photochromism can thus be tuned by simply modifying both the light source and the exposure time, and the Cu content in titania. This is a very rapid and sensitive process. For **Cu−Ti450** under UVA light, there was a 50% reduction of Cu^{2+} in only 12 s, and >95% after 10 min. Under visible light, there is still a large decrease in the Cu^{2+} d−d transition in a relatively short time, with a reduction of ∼25% after just 1 min, ∼ 50% after 5 min, and 80% after 1 h. This signifies that this effect, under UVA or visible light, could be monitored to give detailed and precise information on exposure times, or that small exposure times have a large effect on the tuning of these values, which could be exploited in a new generation of photoactive devices.

This is the first report of such NPs possessing a tunable photochromic property, depending on the light and the exposure time applied, that thus may potentially be used for creating multifunctional and smart coatings (self-cleaning, photocatalytic, antibacterial, photoelectrochemical cells, and sensors).

■ ASSOCIATED CONTENT

Supporting Information

The Supporting Information is available free of charge on the ACS Publications website at DOI: 10.1021/acs.jpcc.5b07160.

Graphical outputs of Rietveld refinement, and WPPM modeling; bimodal size distribution on selected samples, as obtained from the WPPM analysis; digital photographs of sample **2Cu−Ti450**, prior UVA-light irradiation and after 90 min UVA-light exposure; plots of the area of the band due to the Cu^{2+} d−d transition, and the bands due to Cu_2O and Cu^{2+}/TiO_2 IVCT using the visible-light; tables depicting the energy (centroid), band splitting (fwhm), and intensity (area) of the Cu^{2+} d−d transition and Cu_2O and Cu^{2+}/TiO_2 IVCT transitions (PDF)

■ AUTHOR INFORMATION

Corresponding Authors

*Tel.: +351 234 370 041. E-mail: david.tobaldi@ua.pt; david@davidtobaldi.org.

*E-mail: rpullar@ua.pt.

Notes

The authors declare no competing financial interest.

■ ACKNOWLEDGMENTS

D.M.T. is grateful to the ECO-SEE project (funding from the European Union's Seventh Framework Programme for research, technological development and demonstration under grant agreement no 609234). Professors L. D. Carlos and R. A. S. Ferreira (Physics Department and CICECO−Aveiro Institute of Materials, University of Aveiro) are kindly acknowledged for the constructive and fruitful discussions. R.C.P. acknowledges the support of FCT Grant SFRH/BPD/97115/2013. This work was developed in the scope of the project CICECO−Aveiro Institute of Materials (ref. FCT UID/CTM/50011/2013), financed by national funds through the FCT/MEC and when applicable cofinanced by FEDER under the PT2020 Partnership Agreement. M. Ferro and RNME − University of Aveiro, FCT Project REDE/1509/RME/2005−are also acknowledged for HR-TEM analysis. M.L. wants to acknowledge the support of the Italian government with the Futuro in Ricerca project RBFR10CWDA.

■ REFERENCES

(1) Kamat, P. V. Dominance of Metal Oxides in the Era of Nanotechnology. *J. Phys. Chem. Lett.* **2011**, *2*, 839−840.

(2) Chen, X.; Selloni, A. Introduction: Titanium Dioxide (TiO_2) Nanomaterials. *Chem. Rev.* **2014**, *114*, 9281−9282.

(3) Gosbell, I. B. Methicillin-Resistant Staphylococcus Aureus. *Am. J. Clin. Dermatol.* **2004**, *5*, 239−259.

(4) Tong, H.; Ouyang, S.; Bi, Y.; Umezawa, N.; Oshikiri, M.; Ye, J. Nano-Photocatalytic Materials: Possibilities and Challenges. *Adv. Mater.* **2012**, *24*, 229−251.

(5) Zhang, H.; Banfield, J. F. Structural Characteristics and Mechanical and Thermodynamic Properties of Nanocrystalline TiO_2. *Chem. Rev.* **2014**, *114*, 9613−9644.

(6) Ampelli, C.; Passalacqua, R.; Genovese, C.; Perathoner, S.; Centi, G.; Montini, T.; Gombac, V.; Delgado Jaen, J. J.; Fornasiero, P. H_2 Production by Selective Photo-Dehydrogenation of Ethanol in Gas and Liquid Phase on CuO_x/TiO_2 Nanocomposites. *RSC Adv.* **2013**, *3*, 21776.

(7) Maira, A. J.; Lau, W. N.; Lee, C. Y.; Yue, P. L.; Chan, C. K.; Yeung, K. L. Performance of a Membrane-Catalyst for Photocatalytic Oxidation of Volatile Organic Compounds. *Chem. Eng. Sci.* **2003**, *58*, 959−962.

(8) Cao, S.; Yeung, K. L.; Yue, P.-L. An Investigation of Trichloroethylene Photocatalytic Oxidation on Mesoporous Titania-Silica Aerogel Catalysts. *Appl. Catal., B* **2007**, *76*, 64−72.

(9) Herrmann, J.-M.; Duchamp, C.; Karkmaz, M.; Hoai, B. T.; Lachheb, H.; Puzenat, E.; Guillard, C. Environmental Green Chemistry as Defined by Photocatalysis. *J. Hazard. Mater.* **2007**, *146*, 624−629.

(10) Kowal, K.; Wysocka-Król, K.; Kopaczyńska, M.; Dworniczek, E.; Franiczek, R.; Wawrzyńska, M.; Vargová, M.; Zahoran, M.; Rakovský, E.; Kuš, P.; et al. In Situ Photoexcitation of Silver-Doped Titania Nanopowders for Activity against Bacteria and Yeasts. *J. Colloid Interface Sci.* **2011**, *362*, 50−57.

(11) Hajipour, M. J.; Fromm, K. M.; Akbar Ashkarran, A.; Jimenez de Aberasturi, D.; Larramendi, I. R.; de Rojo, T.; Serpooshan, V.; Parak, W. J.; Mahmoudi, M. Antibacterial Properties of Nanoparticles. *Trends Biotechnol.* **2012**, *30*, 499−511.

(12) Tobaldi, D. M.; Piccirillo, C.; Pullar, R. C.; Gualtieri, A. F.; Seabra, M. P.; Castro, P. M. L.; Labrincha, J. A. Silver-Modified Nano-Titania as an Antibacterial Agent and Photocatalyst. *J. Phys. Chem. C* **2014**, *118*, 4751−4766.

(13) Sorar, I.; Pehlivan, E.; Niklasson, G. A.; Granqvist, C. G. Electrochromism of DC Magnetron Sputtered TiO_2 Thin Films: Role of Deposition Parameters. *Sol. Energy Mater. Sol. Cells* **2013**, *115*, 172−180.

(14) Meher, S. R.; Balakrishnan, L. Sol−gel Derived Nanocrystalline TiO_2 Thin Films: A Promising Candidate for Self-Cleaning Smart Window Applications. *Mater. Sci. Semicond. Process.* **2014**, *26*, 251−258.

(15) Granqvist, C. G. *Handbook of Inorganic Electrochromic Materials*; Elsevier: Amsterdam, 1995.

(16) He, T.; Yao, J. Photochromism in Composite and Hybrid Materials Based on Transition-Metal Oxides and Polyoxometalates. *Prog. Mater. Sci.* **2006**, *51*, 810−879.

(17) Ohko, Y.; Tatsuma, T.; Fujii, T.; Naoi, K.; Niwa, C.; Kubota, Y.; Fujishima, A. Multicolour Photochromism of TiO_2 Films Loaded with Silver Nanoparticles. *Nat. Mater.* **2003**, *2*, 29−31.

(18) Naoi, K.; Ohko, Y.; Tatsuma, T. TiO_2 Films Loaded with Silver Nanoparticles: Control of Multicolor Photochromic Behavior. *J. Am. Chem. Soc.* **2004**, *126*, 3664−3668.

(19) Naoi, K.; Ohko, Y.; Tatsuma, T. Switchable Rewritability of Ag-TiO_2 Nanocomposite Films with Multicolor Photochromism. *Chem. Commun.* **2005**, *No. 10*, 1288.

DOI: 10.1021/acs.jpcc.5b07160
J. Phys. Chem. C 2015, 119, 23658−23668

(20) Hutter, E.; Fendler, J. H.; Roy, D. Surface Plasmon Resonance Studies of Gold and Silver Nanoparticles Linked to Gold and Silver Substrates by 2-Aminoethanethiol and 1,6-Hexanedithiol. *J. Phys. Chem. B* **2001**, *105*, 11159−11168.
(21) Tobaldi, D. M.; Pullar, R. C.; Gualtieri, A. F.; Seabra, M. P.; Labrincha, J. A. Phase Composition, Crystal Structure and Microstructure of Silver and Tungsten Doped TiO_2 Nanopowders with Tuneable Photochromic Behaviour. *Acta Mater.* **2013**, *61*, 5571−5585.
(22) Willets, K. A.; Van Duyne, R. P. Localized Surface Plasmon Resonance Spectroscopy and Sensing. *Annu. Rev. Phys. Chem.* **2007**, *58*, 267−297.
(23) Wang, P.; Huang, B.; Dai, Y.; Whangbo, M.-H. Plasmonic Photocatalysts: Harvesting Visible Light with Noble Metal Nanoparticles. *Phys. Chem. Chem. Phys.* **2012**, *14*, 9813.
(24) Gordon, R.; Sinton, D.; Kavanagh, K. L.; Brolo, A. G. A New Generation of Sensors Based on Extraordinary Optical Transmission. *Acc. Chem. Res.* **2008**, *41*, 1049−1057.
(25) Xia, Y.; Halas, N. J. Shape-Controlled Synthesis and Surface Plasmonic Properties of Metallic Nanostructures. *MRS Bull.* **2005**, *30*, 338−348.
(26) Jin, Q.; Fujishima, M.; Iwaszuk, A.; Nolan, M.; Tada, H. Loading Effect in Copper(II) Oxide Cluster-Surface-Modified Titanium(IV) Oxide on Visible- and UV-Light Activities. *J. Phys. Chem. C* **2013**, *117*, 23848−23857.
(27) Ruparelia, J. P.; Chatterjee, A. K.; Duttagupta, S. P.; Mukherji, S. Strain Specificity in Antimicrobial Activity of Silver and Copper Nanoparticles. *Acta Biomater.* **2008**, *4*, 707−716.
(28) Yoon, K.-Y.; Hoon Byeon, J.; Park, J.-H.; Hwang, J. Susceptibility Constants of Escherichia Coli and Bacillus Subtilis to Silver and Copper Nanoparticles. *Sci. Total Environ.* **2007**, *373*, 572−575.
(29) Chan, G. H.; Zhao, J.; Hicks, E. M.; Schatz, G. C.; Van Duyne, R. P. Plasmonic Properties of Copper Nanoparticles Fabricated by Nanosphere Lithography. *Nano Lett.* **2007**, *7*, 1947−1952.
(30) Tobaldi, D. M.; Pullar, R. C.; Gualtieri, A. F.; Seabra, M. P.; Labrincha, J. A. Sol−gel Synthesis, Characterisation and Photocatalytic Activity of Pure, W-, Ag- and W/Ag Co-Doped TiO_2 Nanopowders. *Chem. Eng. J.* **2013**, *214*, 364−375.
(31) Tobaldi, D. M.; Pullar, R. C.; Binions, R.; Belen Jorge, A.; McMillan, P. F.; Saeli, M.; Seabra, M. P.; Labrincha, J. A. Influence of Sol Counter-Ions on the Visible Light Induced Photocatalytic Behaviour of TiO_2 Nanoparticles. *Catal. Sci. Technol.* **2014**, *4*, 2134.
(32) Larson, A. C.; Von Dreele, R. B. *General Structure Analysis System (GSAS)*; Los Alamos National Laboratory Report LAUR: New Mexico, 2004.
(33) Toby, B. H. EXPGUI, a Graphical User Interface for GSAS. *J. Appl. Crystallogr.* **2001**, *34*, 210−213.
(34) Howard, C. J.; Sabine, T. M.; Dickson, F. Structural and Thermal Parameters for Rutile and Anatase. *Acta Crystallogr., Sect. B: Struct. Sci.* **1991**, *47*, 462−468.
(35) Meagher, E. P.; Lager, G. A. Polyhedral Thermal Expansion in the TiO_2 Polymorphs; Refinement of the Crystal Structures of Rutile and Brookite at High Temperature. *Can. Miner.* **1979**, *17*, 77−85.
(36) Scardi, P.; Leoni, M. Whole Powder Pattern Modelling. *Acta Crystallogr., Sect. A: Found. Crystallogr.* **2002**, *58*, 190−200.
(37) Leoni, M.; Confente, T.; Scardi, P. PM2K: A Flexible Program Implementing Whole Powder Pattern Modelling. *Z. Kristallogr. Suppl.* **2006**, *23*, 249−254.
(38) Scardi, P.; Leoni, M. Whole Powder Pattern Modelling: Theory and Applications. In *Springer Ser. Mater. Sci.*; Mittemeijer, E. J., Scardi, P., Eds.; Springer: Berlin, **2004**; Vol. *68*, pp 51−92.
(39) Scardi, P.; Leoni, M. Line Profile Analysis: Pattern Modelling versus Profile Fitting. *J. Appl. Crystallogr.* **2006**, *39*, 24−31.
(40) Klug, H. P.; Alexander, L. E. *X-Ray Diffraction Procedures for Polycrystalline and Amorphous Materials*, 2nd ed..; Wiley: New York, 1974.
(41) Williamson, G. K.; Hall, W. H. X-Ray Line Broadening from Filed Aluminium and Wolfram. *Acta Metall.* **1953**, *1*, 22−31.
(42) Scardi, P.; Leoni, M. Diffraction Whole-Pattern Modelling Study of Anti-Phase Domains in Cu3Au. *Acta Mater.* **2005**, *53*, 5229−5239.
(43) Caglioti, G.; Paoletti, A.; Ricci, F. P. On Resolution and Luminosity of a Neutron Diffraction Spectrometer for Single Crystal Analysis. *Nucl. Instrum. Methods* **1960**, *9*, 195−198.
(44) Marfunin, A. S. *Physics of Minerals and Inorganic Materials: An Introduction*; Springer-Verlag: Berlin, 1979.
(45) Stadelmann, P. JEMS-SAAS. 2014.
(46) Pottier, A.; Chanéac, C.; Tronc, E.; Mazerolles, L.; Jolivet, J.-P. Synthesis of Brookite TiO2 Nanoparticles by Thermolysis of $TiCl_4$ in Strongly Acidic Aqueous Media. *J. Mater. Chem.* **2001**, *11*, 1116−1121.
(47) Shannon, R. D.; Pask, J. A. Kinetics of the Anatase-Rutile Transformation. *J. Am. Ceram. Soc.* **1965**, *48*, 391−398.
(48) Amores, J. M. G.; Escribano, V. S.; Busca, G.; Lorenzelli, V. Solid-State and Surface Chemistry of CuO-TiO_2(anatase) Powders. *J. Mater. Chem.* **1994**, *4*, 965.
(49) Nair, J.; Nair, P.; Mizukami, F.; Oosawa, Y.; Okubo, T. Microstructure and Phase Transformation Behavior of Doped Nanostructured Titania. *Mater. Res. Bull.* **1999**, *34*, 1275−1290.
(50) Yuan, S.; Mériaudeau, P.; Perrichon, V. Catalytic Combustion of Diesel Soot Particles on Copper Catalysts Supported on TiO_2. Effect of Potassium Promoter on the Activity. *Appl. Catal., B* **1994**, *3*, 319−333.
(51) Francisco, M. S. P.; Mastelaro, V. R. Inhibition of the Anatase−Rutile Phase Transformation with Addition of CeO_2 to CuO−TiO_2 System: Raman Spectroscopy, X-Ray Diffraction, and Textural Studies. *Chem. Mater.* **2002**, *14*, 2514−2518.
(52) Burns, A.; Hayes, G.; Li, W.; Hirvonen, J.; Demaree, J. D.; Shah, S. I. Neodymium Ion Dopant Effects on the Phase Transformation in Sol−gel Derived Titania Nanostructures. *Mater. Sci. Eng., B* **2004**, *111*, 150−155.
(53) Thiel, J.; Pakstis, L.; Buzby, S.; Raffi, M.; Ni, C.; Pochan, D. J.; Shah, S. I. Antibacterial Properties of Silver-Doped Titania. *Small* **2007**, *3*, 799−803.
(54) Shannon, R. D. Revised Effective Ionic Radii and Systematic Studies of Interatomic Distances in Halides and Chalcogenides. *Acta Crystallogr., Sect. A: Cryst. Phys., Diffr., Theor. Gen. Crystallogr.* **1976**, *32*, 751−767.
(55) *Spectroscopic Methods in Mineralogy and Geology*; Hawthorne, F. C., Mineralogical Society of America, Eds.; Mineralogical Society of America: Washington, DC, 1988.
(56) Irie, H.; Miura, S.; Kamiya, K.; Hashimoto, K. Efficient Visible Light-Sensitive Photocatalysts: Grafting Cu(II) Ions onto TiO_2 and WO_3 Photocatalysts. *Chem. Phys. Lett.* **2008**, *457*, 202−205.
(57) Banerjee, S.; Chakravorty, D. Optical Absorption by Nanoparticles of Cu_2O. *Europhys. Lett. EPL* **2000**, *52*, 468−473.
(58) Qiu, X.; Miyauchi, M.; Sunada, K.; Minoshima, M.; Liu, M.; Lu, Y.; Li, D.; Shimodaira, Y.; Hosogi, Y.; Kuroda, Y.; et al. Hybrid Cu_xO/TiO_2 Nanocomposites As Risk-Reduction Materials in Indoor Environments. *ACS Nano* **2012**, *6*, 1609−1618.
(59) Dias Filho, N. L. Adsorption of Cu(II) and Co(II) Complexes on a Silica Gel Surface Chemically Modified with 2-Mercaptoimidazole. *Microchim. Acta* **1999**, *130*, 233−240.
(60) Irie, H.; Kamiya, K.; Shibanuma, T.; Miura, S.; Tryk, D. A.; Yokoyama, T.; Hashimoto, K. Visible Light-Sensitive Cu(II)-Grafted TiO_2 Photocatalysts: Activities and X-Ray Absorption Fine Structure Analyses. *J. Phys. Chem. C* **2009**, *113*, 10761−10766.
(61) Fujishima, A.; Honda, K. Electrochemical Photolysis of Water at a Semiconductor Electrode. *Nature* **1972**, *238*, 37−38.
(62) Cruciani, G.; Ardit, M.; Dondi, M.; Matteucci, F.; Blosi, M.; Dalconi, M. C.; Albonetti, S. Structural Relaxation around Cr^{3+} in $YAlO_3$ − $YCrO_3$ Perovskites from Electron Absorption Spectra. *J. Phys. Chem. A* **2009**, *113*, 13772−13778.
(63) Ghauch, A.; Turnar, C.; Fachinger, C.; Rima, J.; Charef, A.; Suptil, J.; Martin-Bouyer, M. Use of Diffuse Reflectance Spectrometry in Spot Test Reactions for Quantitative Determination of Cations in Water. *Chemosphere* **2000**, *40*, 1327−1333.
(64) Kafizas, A.; Dunnill, C. W.; Parkin, I. P. The Relationship between Photocatalytic Activity and Photochromic State of Nanoparticulate Silver Surface Loaded Titanium Dioxide Thin-Films. *Phys. Chem. Chem. Phys.* **2011**, *13*, 13827.

DOI: 10.1021/acs.jpcc.5b07160
J. Phys. Chem. C 2015, 119, 23658−23668